Supplementary Information

Lilac flower-shaped $ZnCo_2O_4$ electrocatalyst for efficient methanol oxidation and oxygen reduction reactions in alkaline medium

T.V. M. Sreekanth, P.C. Nagajyothi, K. C. Devarayapalli, J. Shim, K. Yoo*

School of Mechanical Engineering, Yeungnam University, Gyeongsan-38541,

Republic of Korea

* Corresponding author: Prof. K. Yoo, Email: kisooyoo@yu.ac.kr

Materials and methods

$ZnCo_2O_4$ LFs were effectively synthesized by a microwave-assisted method. In a typical synthesis, 50 mL each of deionized water (DIW) and ethanol were taken in a 250 mL beaker, then 4 mM, 2 mM, 10 mM and 12 mM of $Co(NO_3)_2 \cdot 6H_2O$, $Zn(NO_3)_2 \cdot 6H_2O$, NH_4F, and Hexamethylenetetramine (HMT), respectively, were added. The sample mixture was stirred until completely dissolved, forming a clear pink solution. The reaction mixture was then transferred to a Teflon-lined autoclave, and fixed in a microwave chamber (Analytikjena TOPwave-CX-100, Germany), at a constant temperature of 160 °C, for 15 min. After natural cooling to RT, the solid sample was collected by centrifuging at 10000 rpm for 10 min, washed three times with DIW and ethanol (EtOH), and then dried at 80 °C overnight. To get a pure phase of $ZnCo_2O_4$ LFs, the powder was then annealed, at 400 °C in air, for 4 h, at a ramping rate of 5 °C min^{-1}.

Characterization

The crystallinity of the as-prepared sample was measured using powder XRD (PXRD; PANalytical X-Pert PRO, USA) with a Cu Kα radiation source (λ = 1.5405 Å). The elemental composition was measured using XPS (XPS; K-alpha, Thermo Scientific, USA) with Al Kα radiation (1486.6 eV) technique. The morphology of the samples was investigated by SEM, with a field emission gun (4800, Hitachi, Japan) and HRTEM (Tecnai G2 F20 S-TWIN, USA) with a 200 kV field emission gun in Schottky mode. BET surface area and the BJH pore volume and

size were measured from N_2 adsorption and desorption curves of the synthesized samples, which were recorded on an automatic surface analyzer (3-Flex, Micrometrics, USA).

Electrode preparation and electro-catalytic performance measurement

The electro-catalytic MOR was carried out with an electrochemical station (Biologic, VSM SP-3, and South Korea) using different electrochemical methods, including CV and EIS, at ambient temperature. The electrochemical performance was investigated using the $ZnCo_2O_4$ LFs on nickel foam (NF) electrode, as the working electrode, Ag/AgCl as the reference electrode, and Pt as the counter electrode. For this, a slurry was prepared by mixing 80% $ZnCo_2O_4$ LFs, 10% Ketjen black, and 10% PVDF, which was then added to 100 µL of n-methyl-2-pyrrolidone, and sonicated for 60 min, after which, 50 µL slurry was added to the NF. 1.0 M solutions of KOH, with and without different concentrations of methanol (0.5–5.0 M), were used as an electrolyte.

The CV was recorded for $ZnCo_2O_4$LFs at scan rates ranging between 5–100 mVs^{-1}, and for MOR study, we fixed the scan rate at 50 mVs^{-1}, in the potential range 0.0–0.6 V. EIS measurements were carried out at 10 mV voltage amplitudes, over the frequency range of 1 Hz to 1 MHz. The mass loading of active materials on the NF, for MOR measurements, was ~5.0 mg.

The electro-catalytic ORR was carried out using an RRDE (RRDE-3A, ALS, Co., Ltd., Tokyo, Japan) with Biologic, VSM SP-3, using CV and linear seep voltammetry (LSV), with a conventional, three-electrode system in N_2- and O_2-saturated, 0.1 M KOH aqueous electrolyte solution. Glassy carbon disk (GCD; RRDE-3A, 4.0 mm disk diameter) was used as the working electrode, and the slurry was prepared by mixing 15 µL DIW and 80 µL isopropyl alcohol with 2.5 mg of active catalyst ($ZnCo_2O_4$LFs). After this, 5 µL Nafion solution (5.0 wt%) was added, and sonicated for 40 min at a constant temperature to form a homogeneous ink. Then 7 µL catalyst ink was loaded onto the GCD and dried at ambient temperature. Before studying ORR activity in the RRDE, high-purity O_2 gas was purged, for 30 min, to achieve O_2saturation between the electrolytes. CV measurements were performed at a scan rate 10 mVs^{-1}, in the range of 0.0–1.2 V, vs. a reversible hydrogen electrode (RHE), and for LSV, measurements were performed at a scan rate 10 mVs^{-1}, in the range of 0.0–1.0 V, vs. RHE [1]. Koutecky–Levich

plots (K–L plots: J^{-1} vs $\omega^{-1/2}$) were generated at numerous electrode potentials, to calculate the number of electrons (e-) transferred (n) based on the K–L equation [2]:

$$\frac{1}{j} = \frac{1}{j_L} + \frac{1}{j_K} = \frac{1}{B\omega^{1/2}} + \frac{1}{j_k} \quad (1)$$

$$B = 0.62\, nFC_0(D_0)^{3/2}\upsilon^{1/6} \quad (2)$$

$$j_k = nFkC_0 \quad (3)$$

where j (mA.cm^{-2}) denotes the measured current density, j_K and j_L are the kinetic and diffusion-limiting current densities, respectively, ω is the angular velocity of the rotating disk ($\omega = 2\pi N$, where N is the linear rotating speed in rpm), and n represents the overall number of electrons transferred in ORR, F stands for the Faraday constant (96485 °C mol^{-1}). Also, C_0 is the bulk concentration of O_2 (1.2×10^{-6} mol cm^{-3}), D_0 is the diffusion coefficient of O_2 (1.9×10^{-5} cm^2 s^{-1}), υ is the kinematic viscosity of the electrolyte (0.01 cm^2 s^{-1}), and k related to the electron (e$^-$) transfer rate constant. Using Eq. (1)–(3), n can be calculated from the slope and intercept of the linear fitted K–L curves (J^{-1} vs $\omega^{-1/2}$). The electrode potential is transformed from Ag/AgCl electrode potential to RHE potential by using the standard conversion formula [2]

$$E\,(RHE) = E\,(Ag/AgCl) + 0.059\,pH + E^0\,(Ag/AgCl) \quad (4)$$

where E^0 (Ag/AgCl) = 0.197 V.

Calibration of collection efficiency (Nc)

The collection efficiency (N_c) of the electrode was calibrated using the RRDE [3]. Using 0.1 M KOH, with 4 mmol $K_3Fe(CN)_6$, a typical compound for the determination of collection efficiency, the $ZnCo_2O_4$LFs electrode was used to determine N_c. The ring and disk currents were applied at the scan rate of 20 mVs^{-1}, at room temperature. The voltage of the disk and ring were set to 0.1 V and 1.5 V, respectively, and the reactions taking place on the disk and ring were as shown in (5) and (6):

Disk:

$$Fe(CN)_6^{3-} + e^- \rightarrow Fe(CN)_6^{4-} \quad (5)$$

Ring:

$$Fe(CN)_6^{4-} \rightarrow Fe(CN)_6^{3-} + e^- \quad (6)$$

The measurement lasted 70 s, and the disk and ring currents (I_d and I_r) for the last 10 s were averaged. The measurements were repeated once with the disk disconnected. The ring current (I_{r0}) for the last 10 s was also averaged, and I_{r0} included all anodic currents that were not from $Fe(CN)_6^{4-}$ reduced on the disk (they may be related to the oxidation of water, free$Fe(CN)_6^{4-}$, or any impurities). The N_c value was calculated using (7):

$$N_c = \frac{I_{r-I_{ro}}}{I_d} \quad (7)$$

H_2O_2 and the number of electrons transferred (n) were calculated by the following relation:

$$H_2O_2 = 200 \times \frac{I_R/N}{I_D + I_R/N} \quad (8)$$

$$n = 4 \times \frac{I_D}{I_D + I_R/N} \quad (9)$$

where I_D, I_R and N are disk current, ring current and collection efficiency (0.359), respectively.

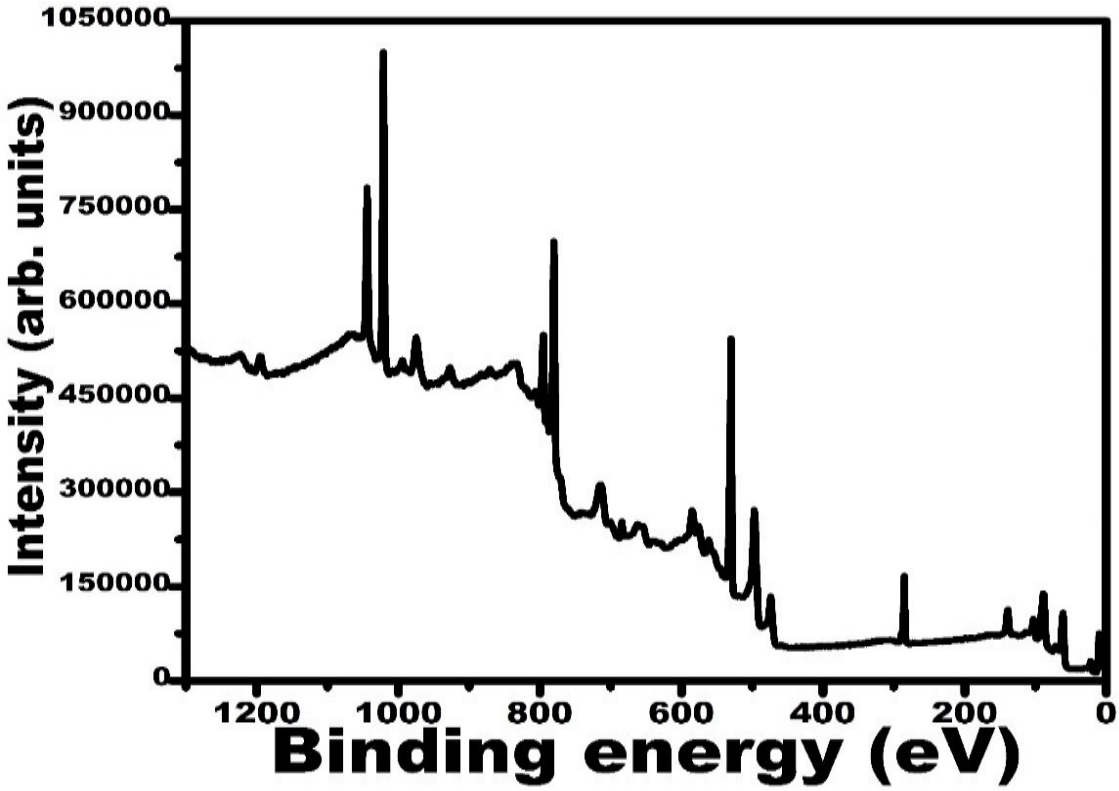

Figure S1 Survey scan spectrum of $ZnCo_2O_4$ LFs

BET analysis

Nitrogen (N_2) adsorption/desorption isotherms were measured to study the BET specific surface area and pore size distribution of the $ZnCo_2O_4$ LFs and the results were shown in Figure.S1, the BET surface area of $ZnCo_2O_4$ LFs was 23.30 m^2 g^{-1}, and the BJH pore volume of $ZnCo_2O_4$ LFs was 0.058 cm^3 g^{-1}.

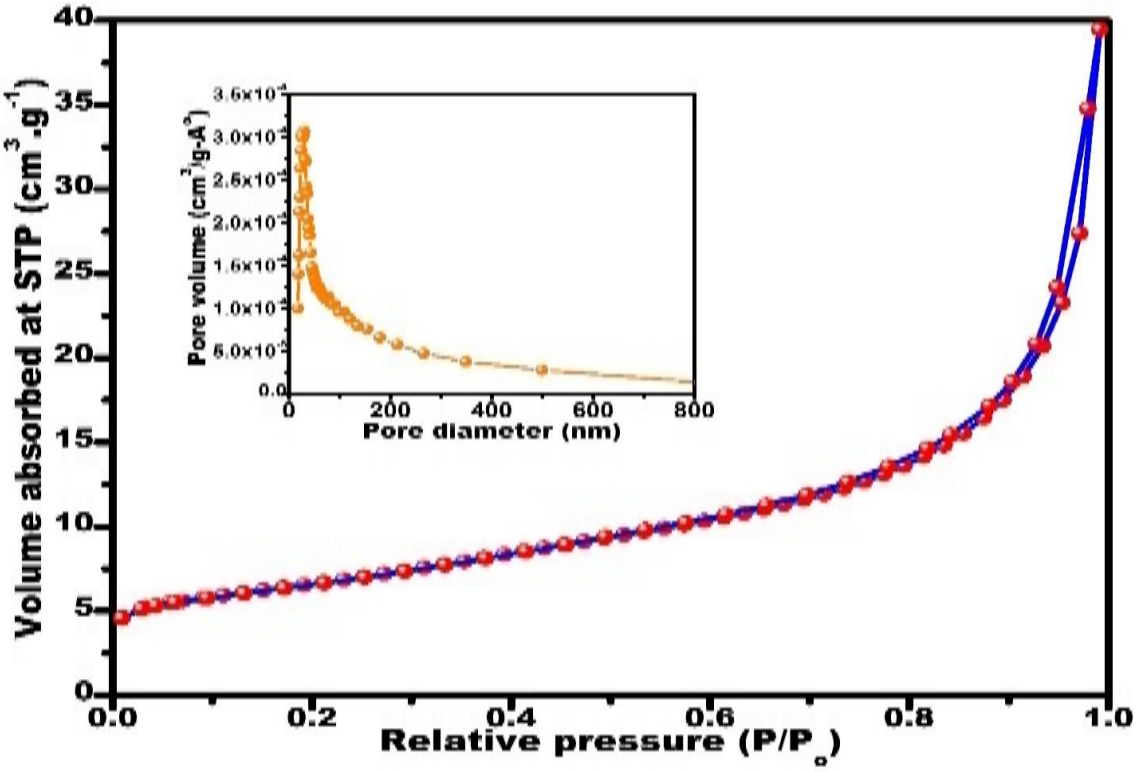

Figure S2 Nitrogen adsorption-desorption isotherms plots and corresponding BJH pore size distributions (insets) of $ZnCo_2O_4$ LFs

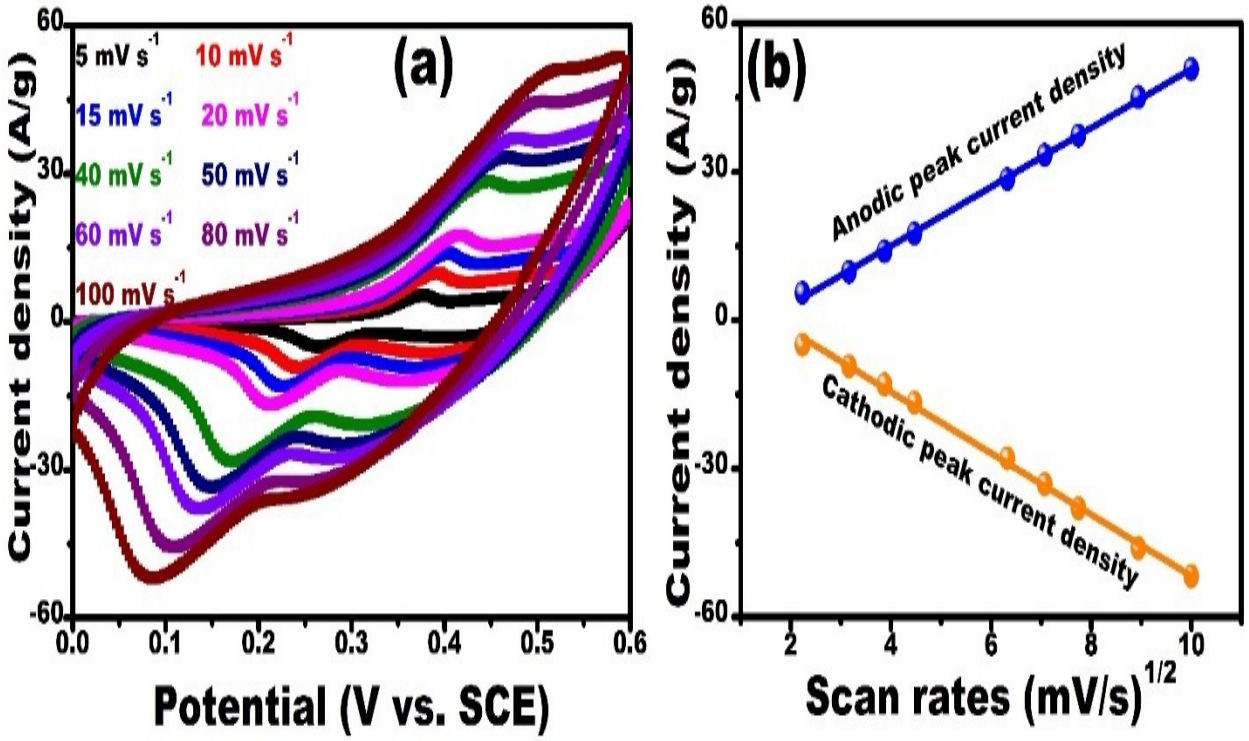

Figure S3 CV curves of $ZnCo_2O_4$ LFs (a) and represents the relationship of the anodic and cathodic peak currents vs. scan rates of $ZnCo_2O_4$ LFs

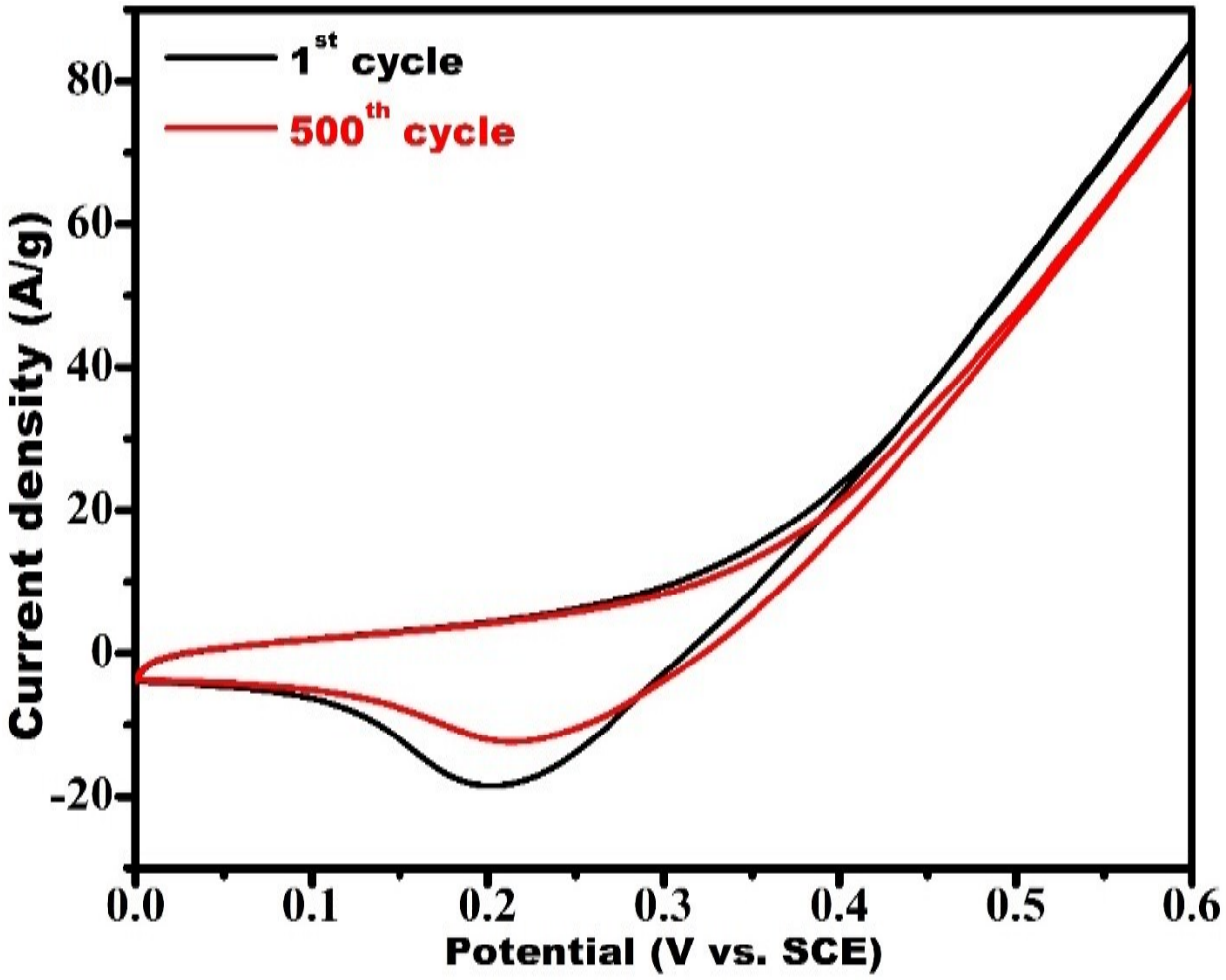

Figure S4 CV graph of the $ZnCo_2O_4$ LFs at a scan rate of 50 mVs^{-1} in a 1.0 M KOH with 0.5 M MeOH for different cycle numbers

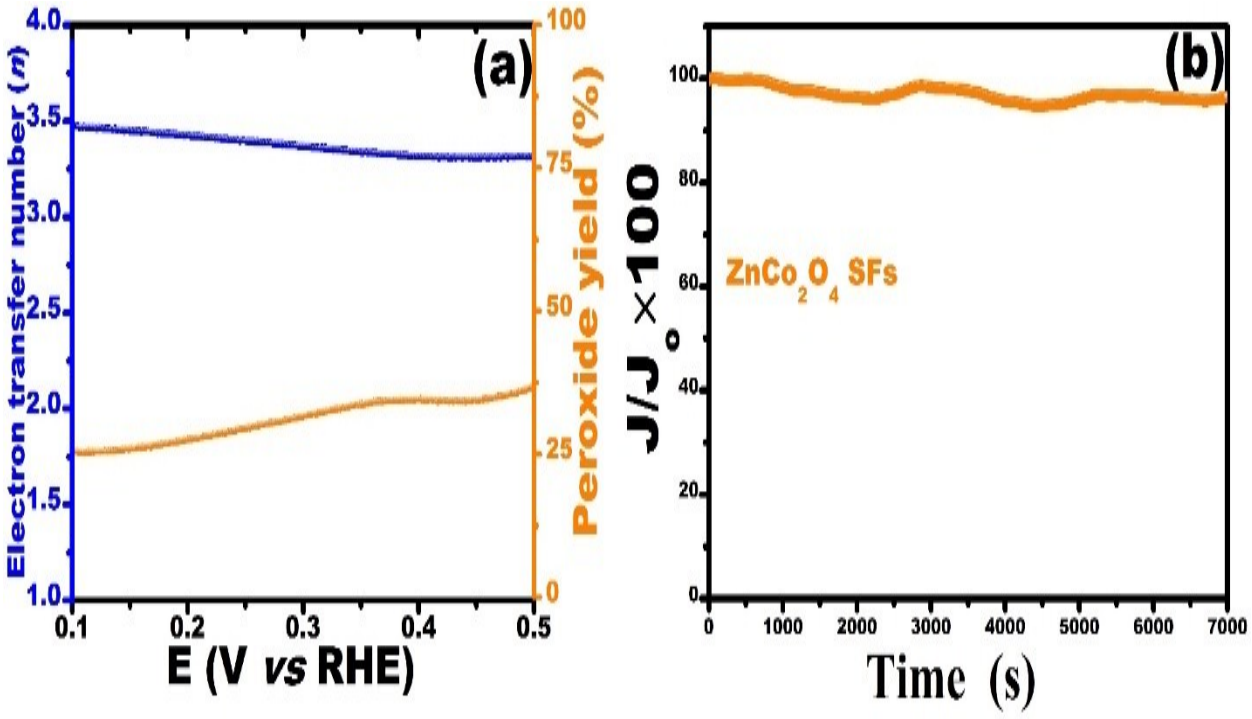

Figure S5. The electron transfer number (n) and peroxide yield (%) of $ZnCo_2O_4$ LFs at various potentials based on the corresponding RRDE data (a) and current-time chronoamperometric (CA) responses for ORR on $ZnCo_2O_4$ LFs catalyst in O_2-saturated 0.1 M KOH electrolyte.

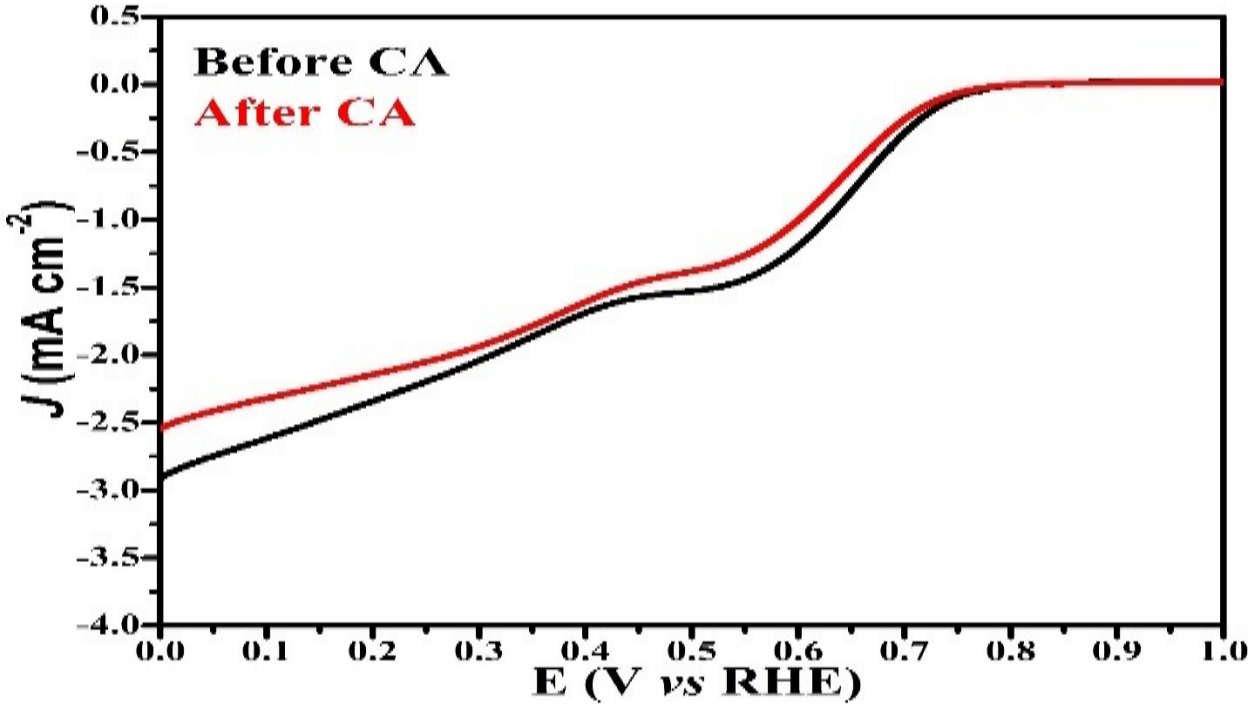

Figure S6. LSV curves of $ZnCo_2O_4$ LFs at a rotation rate of 1600 rpm in the O_2-saturated 0.1 M KOH electrolyte at a scan rate of 10 mVs^{-1} before polarization and after polarization.

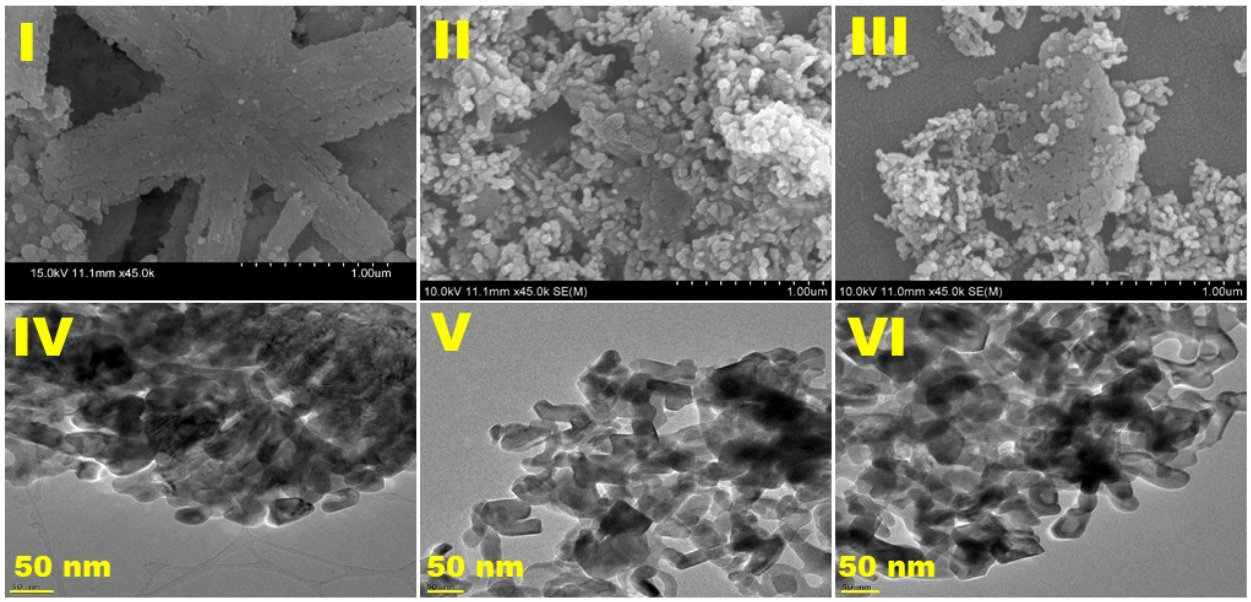

Figure S7. Morphologies of the electrocatalyst, SEM images of $ZnCo_2O_4$ LFs, original (I), post-MOR (II), and post-ORR (III), respectively. HR-TEM images of $ZnCo_2O_4$ LFs, original (I), post-MOR (II), and post-ORR (III), respectively.

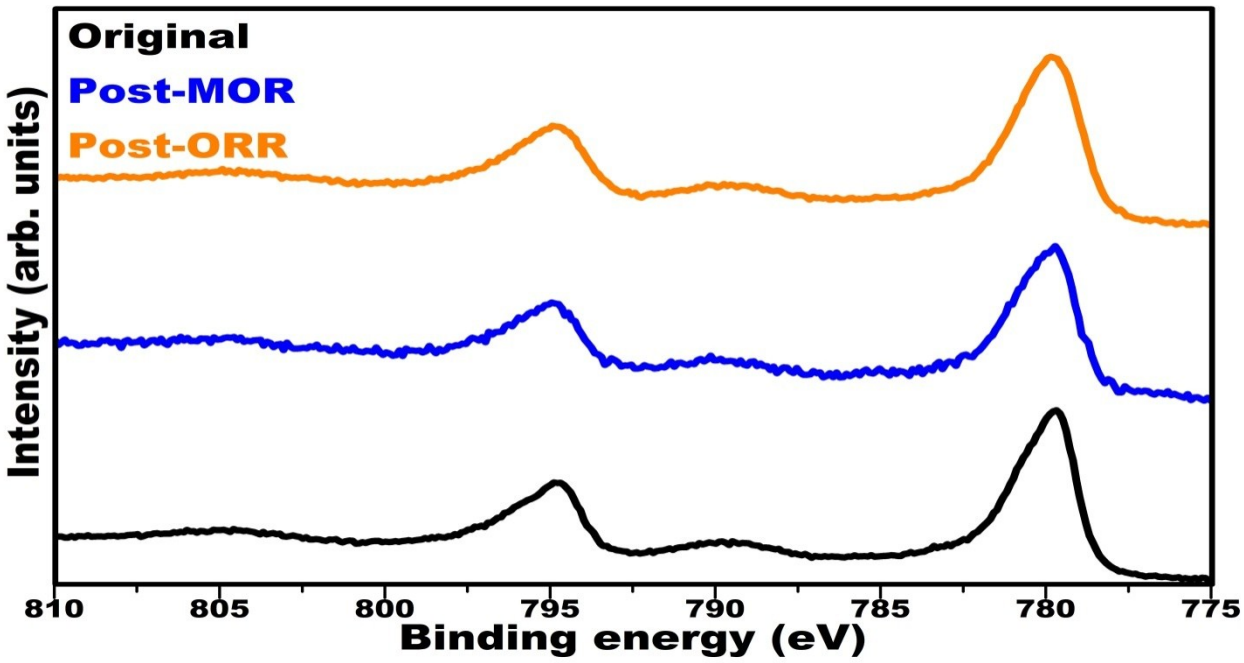

Figure S8. High-resolution XPS spectrum of Cobalt 2p in the electrocatalyst of $ZnCo_2O_4$ LFs original, post-MOR, and post-ORR.

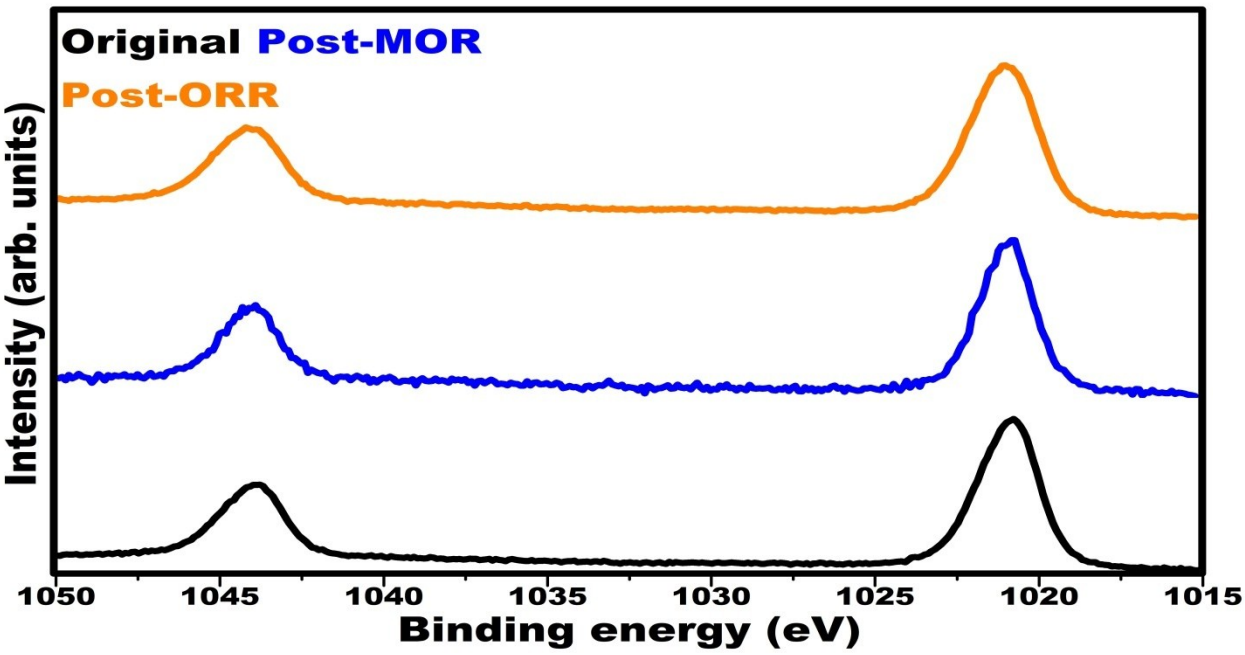

Figure S9. High-resolution XPS spectrum of Zinc 2p in the electrocatalyst of $ZnCo_2O_4$ LFs original, post-MOR, and post-ORR.

Table-S1. Influence of methanol concentration on the current density in MOR with the $ZnCo_2O_4$ LFs electrode.

Methanol concentration (M)	Current density (A/g)
1.0 KOH	36.2
0.5	84.5
1.0	100.7
2.0	106.0
3.0	110.7
4.0	113.0
5.0	118.0

Table-S2. Comparisons of MOR reaction

Catalyst	Substrate	Electrolyte	MOR activity	Ref
$CuCo_2O_4$	Cu foam	1.0 M KOH	24.5 A/g	[4]
$NICo_2O_4/MWCNT_S$	GC	0.1 M KOH	327 mA/cm^2	[5]
$CuCo_2O_4$	NF	1.0 M KOH	45 mA/cm^2	[6]
$ZnCo_2O_4$	NF	1.0 M KOH	105 A/g	[7]
$ZnCo_2O_4$	NF	1.0 M KOH	223.3 mA/cm^2	[8]
$ZnCo_2O_4$	NF	1.0 M KOH	149 mA/cm^2	[9]
$ZnCo_2O_4$	NF	1.0 M KOH	84.5 A/g	This work

Table-S3. Comparisons of ORR reaction

Catalyst	ORR Onset potential [V vs. RHE]	Half-wave potential [$E_{1/2}$ V vs. RHE]	Electrolyte	Ref
Co_3O_4	0.78	0.56	0.1 M KOH	[10]
$MnCo_2O_4$	0.84	0.59		
Co-BTC@AC	0.63	0.5	0.1 M KOH	[11]
Co_3O_4 nanorods	0.90	---	1.0 M KOH	[12]
$ZnCo_2O_4$	0.81	0.75	1.0 M KOH	[13]
RGO-$ZnCo_2O_4$	0.95	0.87		
$ZnCo_2O_4$	0.80	0.69	1.0 M KOH	This work

References

1 Y. Xu, W. Bian, J. Wu, J. H. Tian, R. Yang, Preparation and electrocatalytic activity of 3D hierarchical porous spinel $CoFe_2O_4$ hollow nanospheres as efficient catalyst for oxygen reduction reaction and oxygen evolution reaction. *Electrochi. Acta*2015, **151**, 276-283.

2 S. Chakrabarthy, A. Mukherjee, W. N. Su, S. Basu, Improved bi-functional ORR and OER catalytic activity of reduced graphene oxide supported $ZnCo_2O_4$ microsphere. *Int. J. Hydrogen Energy,*2019, **44**, 1565-1578.

3 U. A. Paulus, T. J. Schmidt, H. A. Gasteiger, R. J. Behm, Oxygen reduction on a high-surface area Pt/Vulcan carbon catalyst: a thin-film rotating ring-disk electrode study. *J. Electroanal Chem.*2001, **495**, 134-145.

4 J. Cheng, H. Yan, Y. Lu, K. Qiu, X. Hou, J. Xu, L. Han, X. Liu, J. K. Kim, Y. Luo, Mesoporous $CuCo_2O_4$ nanograsses as multifunctional electrodes for supercapacitors and electro-catalysts. *J. Mat. Chem. A,*2015,**3**, 9769–9776.

5 T. Ko, K. Devarayan, M. Seo, H. Y. Kim, B. S. Kim, Facile synthesis of core/shell-like $NiCo_2O_4$-decorated MWCNTs and its excellent electrocatalytic activity for methanol oxidation. *Sci. Reports*,2016, **6**, 20313.

6 R. N. Singh, T. Sharma, A. Singh, D. M. Anindita, Electrocatalytic activities of nano-sized spinel-type $Cu_xCo_{3-x}O_4$ ($0 \leq X \leq 1$) for methanol oxidation in alkaline solutions. *Int. J. Electrochem. Sci.* 2007,**2**, 762–777.

7 H. S. Jadhav, A. Roy, W. J. Chung, J. G. Seo, Growth of urchin-like $ZnCo_2O_4$ microspheres on nickel foam as a binder-free electrode for high-performance supercapacitor and methanol electro-oxidation. *Electrochi. Acta*,2017, **246**, 941–950.

8 R. Shi, Y. Zhang, Z. Wang, Facile synthesis of a $ZnCo_2O_4$ electrocatalyst with three-dimensionalarchitecture for methanol oxidation. *J. Alloys Comp.*2019, **810**, 151879.

9 T. V. M. Sreekanth, R. Ramaraghavulu, S. V. Prabhakar Vattikuti, J. Shim, K. Yoo, Microwave synthesis: $ZnCo_2O_4$ NPs as an efficient electrocatalyst in the methanol oxidation reaction. *Mat. Lett.*2019, **253**, 450-453.

10 X. He, F. Yin, S. Yuan, N. Liu, X. Huang, Hybrid spinel oxides/N-doped reduced graphene oxide as highly-active bifunctional electrocatalysts for oxygen reduction/evolution reactions, *Chemelectrochem*, 2016, **3**, 1107-1115.

11 S. Gonen, O. Lori, G. cohene-Taguri, L. Elbaz, Metal organic frameworks as a catalyst for oxygen reduction: an unexpected outcome of a highly active Mn-MOF-based catalyst incorporated in activated carbon, *Nanoscale*, 2018, **10**, 9634-9641.

12 J. Xu, P. Gao, T.S. Zhao, Non-precious Co_3O_4 nano-rod electrocatalyst for oxygen reduction reaction in anion-exchange membrane fuel cells, *Energ Environ Sci*, 2012, 5, 5333-5339.

13 S. Chakrabarty, A. Mukherjee, W-N Su, S. Basu, Improved bi-functional ORR and OER catalytic activity of reduced graphene oxide supported $ZnCo_2O_4$ microsphere, *Int. J. Hydrogen. Energ.*2019, **44**, 1565-1578.